Elastic, charge-exchange, and total K^-p cross sections in the momentum range 220 to 470 MeV/c*

Terry S. Mast, Margaret Alston-Garnjost, Roger O. Bangerter, Angela S. Barbaro-Galtieri, Frank T. Solmitz, and Robert D. Tripp

Lawrence Berkeley Laboratory, University of California, Berkeley, California 94720

(Received 11 December 1975)

An analysis has been made of 64 600 events of the type $K^-p \to K^-p$ and 22 800 events of the type $K^-p \to \bar{K}^0 n$ in the Berkeley 25-in. hydrogen bubble chamber. Differential cross sections have been measured in intervals of 10 MeV/c over the momentum range 220 to 470 MeV/c. Legendre-polynomial fits to the distributions have been made, and the coefficients show structure from the resonant D-wave [$\Lambda(1520)$] and background S and P waves. No new structure is observed. The total K^-p cross section determined from measurements of all final states seen in this exposure is also presented.

I. INTRODUCTION

This paper is one of a series of papers describing a detailed study of the K^-p channel in the region of the $\Lambda(1520)$.[1] The results on the elastic and charge-exchange final states are presented here. Samples of 64 600 events of the type $K^-p \to \bar{K}^0 n$ were obtained in the Berkeley 25-in. hydrogen bubble chamber. The incident momenta range from 220 to 470 MeV/c.

In Sec. II we describe the experimental procedures and the corrections applied to the data to account for scanning and measuring losses. Section III presents the cross sections for these channels and the results of Legendre-polynomial fits to the production angular distributions. The sum of the cross sections for the elastic and charge-exchange reactions and reactions producing hyperons measured in the same exposure[1] yield new K^-p total cross sections.

II. EXPERIMENTAL PROCEDURES

From an exposure of the Berkeley 25-in. hydrogen bubble chamber to a K^- beam we have obtained 1.3×10^6 pictures. The beam has been fully described elsewhere.[2] Typically each picture contained six K^- tracks and two background tracks. The background consisted of pions, muons, and some electrons. Background tracks had close to minimum ionization and were thus easily distinguished from the K^- tracks, which at our momentum have about three times minimum ionization.

By movement of the target and by use of a beryllium beam degrader, we are able to obtain K^- momenta between 220 and 470 MeV/c. The data were taken with 24 different beam settings. However, most of the path length (Fig. 1) occurs

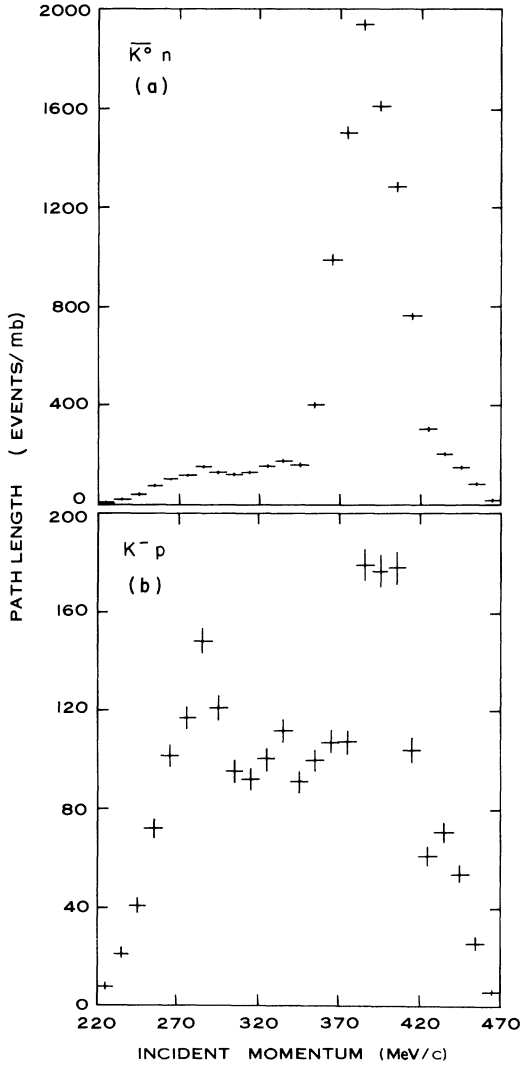

FIG. 1. Path length (events/mb) versus incident K^- momentum (MeV/c) for (a) charge-exchange and (b) elastic events.

close to 395 MeV/c, the momentum required to form the $\Lambda(1520)$.[3]

A. The $\bar{K}^0 n$ final state

The film was scanned for all topologies, including those with a zero prong and vee. The path-length distribution determined from τ decays of the beam[4] is shown in Fig. 1(a). On the basis of ionization the scanners distinguished between vees from the decay $\bar{K}^0 \to \pi^+\pi^-$ and those from the decay $\Lambda \to p\pi^0$. All of the film was scanned once, 38% was scanned twice, and 7% was scanned three times. All events within a restricted fiducial volume were measured with the Spiral Reader or Franckenstein measuring projectors. The kinematic reconstruction and fits to reaction hypotheses were performed with the programs TVGP and SQUAW. The vee for events scanned as $\bar{K}^0$ (Λ) was first fitted to the decay $\bar{K}^0 \to \pi^+\pi^-$ ($\Lambda \to p\pi^0$). The incident beam was used to determine the direction of the neutral, making this a three-constraint fit. If the fit to the decay failed then the opposite-type vee was tried. If both failed then fits to three-body $\bar{K}^0$ decays were tried. Those events which passed a three-constraint decay fit were then fitted to the production and decay:

$$K^- p \to \bar{K}^0 n, \quad \bar{K}^0 \to \pi^+\pi^-, \tag{1}$$

$$K^- p \to \Lambda + \text{missing mass}, \quad \Lambda \to p\pi^0. \tag{2}$$

Events which failed to fit any reaction hypothesis were remeasured until 94% of those scanned as $\bar{K}^0$ and 96% of those scanned as Λ passed. The remaining events were generally unmeasureable owing to the obscuration of a track of the presence of a very short track.

Of those events scanned as $\bar{K}^0$, 6.1% has a better confidence level for a fit to the Λ production and decay. Of those scanned as Λ, 1.4% had a better fit to the $\bar{K}^0$ production and decay.

Only those events which had a confidence level greater than 0.01 were accepted for further analysis. This sample included 29 109 events which fitted only reaction (1), 70 815 events which fitted only reaction (2), and 824 events which fitted both reactions. Comparison of the confidence levels for those events fitting both reactions showed that in most cases one of the two fits was much preferred. An ambiguous event was considered to be the preferred reaction if the confidence-level ratio for the fits was greater than 5.0. Reexamination of a sample of these events shows this to be a good criterion. Of the 824 events

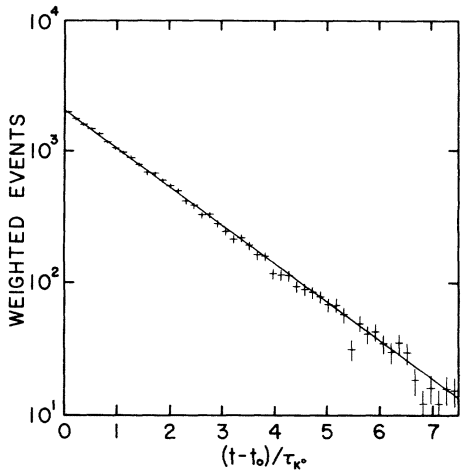

FIG. 2. Distribution of $\bar{K}^0$ lifetimes shifted by the cut imposed to remove the effect of the loss of short-track $\bar{K}^0$'s.

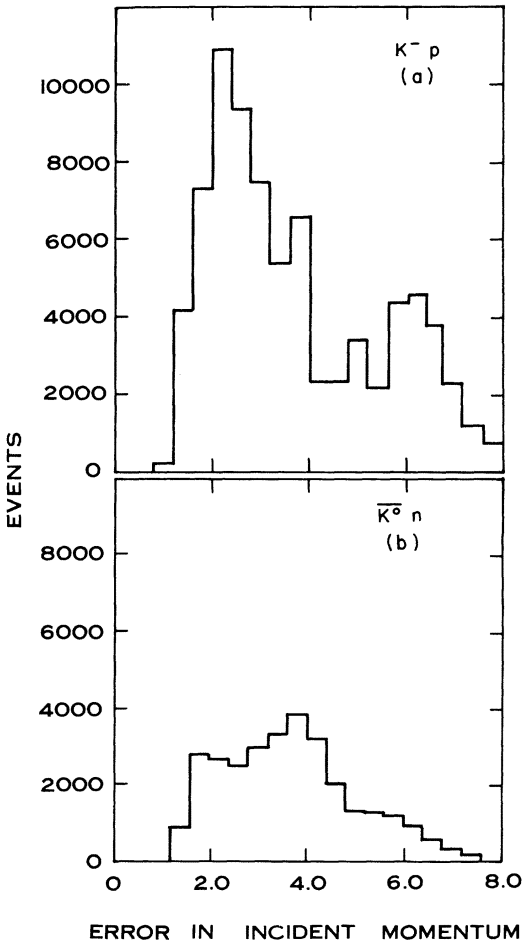

FIG. 3. Distribution of the error in incident momentum resulting from the kinematic fitting of the (a) elastic and (b) charge-exchange events.

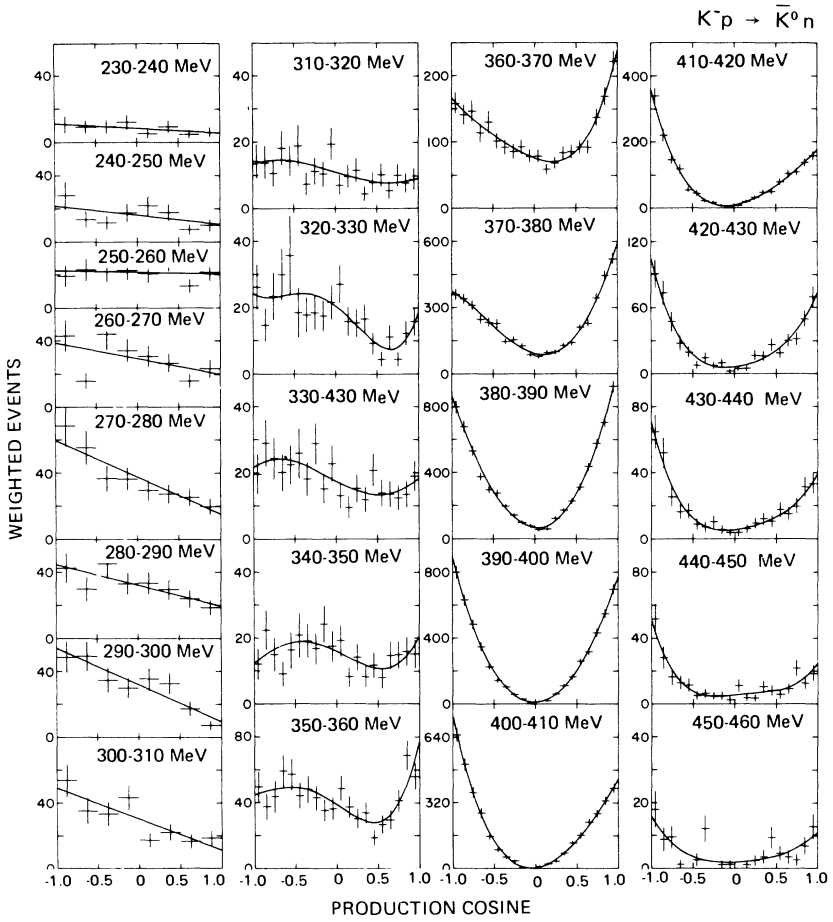

FIG. 4. The production-cosine distributions for the charge-exchange reaction $K^-p \to \bar{K}^0 n$ for events binned in intervals of 10 MeV/c incident K^- momentum. The curves are from the fits to Legendre polynomials described in the text.

82 were accepted as $\bar{K}^0$ events, 712 as Λ events. The remaining 30 truly ambiguous events were simply eliminated from the sample since the number was negligible.

To ensure sufficient track lengths for a good measurement of the $\bar{K}^0$ momentum, further restrictions were made on the fiducial volumes for the production and decay vertices. These reduced the sample of $\bar{K}^0$ events to 26 235 events. To account for a scanning loss of short-track $\bar{K}^0$'s, all events with a projected length less than 2.0 mm were eliminated and the remaining 22 829 events were weighted to account for the cut. The weighting also accounted for loss due to escape from the decay vertex fiducial volume. The mean weight was 1.27. Further losses were investigated by looking at the distribution of the decay π^+ in the $\bar{K}^0$ rest frame. Anisotropy in this distribution was found coming from the loss of events where the $\bar{K}^0$ decay plane is seen edge-on by the scanner and events where the π^+ travels along the $\bar{K}^0$ line of flight. A section of the decay distribution with highly visible events was assumed to have 100% detection efficiency. A comparison of the density of events within and outside this section yielded a weight to account for the losses. This correction yielded a final sample of 30 697 weighted events with a mean weight of 1.34.

The lifetime distribution of the $\bar{K}^0$ is shown in Fig. 2. In order to remove the effect of the cut on short-track $\bar{K}^0$'s the events have been plotted as a function of $t - t_0$ in units of the known $\bar{K}^0$ lifetime. For each event, t_0 is given by 2.0 mm/$\eta c\tau_{K^0} \cos\lambda$, where η is the ratio of the $\bar{K}^0$ momentum to its mass and λ is the dip angle. The distribution is consistent with the line corresponding to the known

lifetime (0.866×10^{-10} sec).[5] Figure 3(b) shows the distribution of errors in the incident K^- momentum produced by the SQUAW fit.

B. The K^-p final state

The two-prong topology was scanned for in 17% of the film. The sections chosen for scanning for this topology were distributed in incident momentum, and the pathlength distribution was determined from τ decays of the beam as shown in Fig. 1(b). 62% of this film was scanned a second time and 11% was scanned for a third time. About one-fourth of the incident beam consisted of negative pions, muons, or electrons, and scanners excluded π^-p interactions on the basis of ionization. In addition, the scanners were asked to flag the outgoing positive track as "proton" or "nonproton" on the basis of ionization; 5% were flagged as "nonproton."

All scanned events were measured and fitted to a variety of πp and Kp reaction hypotheses. Since the center-of-mass energy is low the number of possible final states is limited. Up to 16 reaction hypotheses were tried. These included elastic scatterings, pion production, and hyperon production (where the hyperon or its decay products had zero-length tracks and could thereby simulate a K^-p elastic topology). Events which failed to fit at least one hypothesis with a confidence level greater than 0.01 were remeasured until 98% passed this criterion. To allow sufficient track length for a good measurement, only events within a restricted fiducial volume were accepted for further analysis. This sample consisted of about 80400 events. Of these 80.7% fitted only one reaction hypothesis, 18.8% fitted two reaction hypotheses, and 0.005% fitted three or more reaction hypotheses.

To reduce the ambiguities a cut was made on the proton lab momentum. Events with a proton lab momentum less than 100 MeV/c (corresponding to a track length of 2.8 mm) were eliminated. This cut corresponds to a cut in the center-of-mass production cosine which varies from 0.765 at 225 MeV/c to 0.930 at 465 MeV/c.

Of those events fitting only one hypothesis, 85% fitted $K^-p\to K^-p$. The remaining 15% of the events were studied to see if they were poorly measured K^-p elastic scatterings. Many of these fitted πp elastic scattering. Where track ionization information was available from the Spiral Reader measurement, this was used to estimate the number of K^-p elastic events in the sample. About 1% of the 15% did have a low confidence level (<0.01) for the K^-p elastic hypothesis, and these low-confidence-level events were included in the final sample. On the basis of ionization information and reexamination of the events on the scan table we estimate an additional 2% of the 15% are true K^-p elastic scatterings without a fit to that hypothesis.

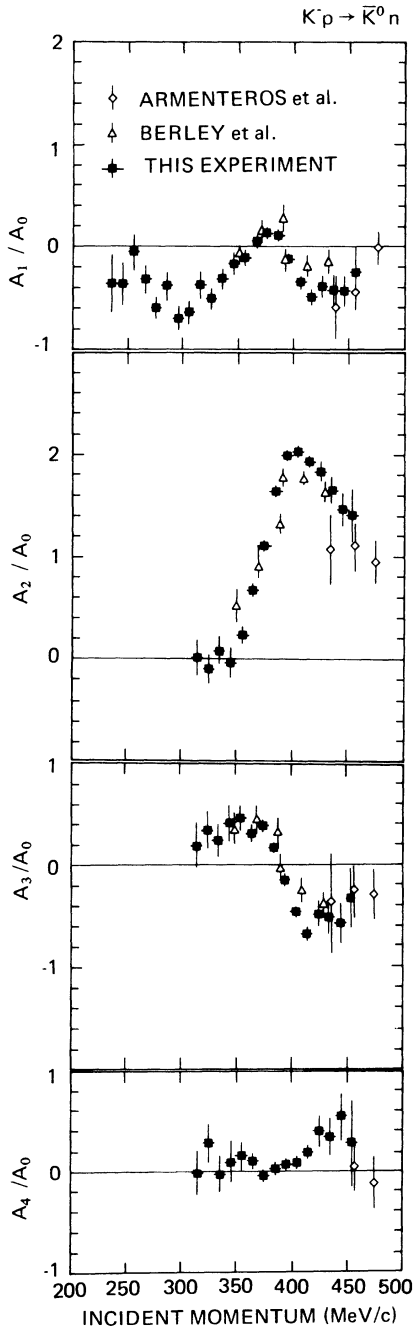

FIG. 5. Legendre coefficients A_l/A_0 ($l=1,4$) as a function of incident momentum for the angular distribution in the charge-exchange reaction $K^-p\to\bar{K}^0n$. The data of Berley *et al.* (Ref. 7) and Armenteros *et al.* (Ref. 10) are shown for comparison.

TABLE I. Differential cross sections (mb/sr) for $K^-p \to \bar{K}^0 n$.

Center of bin (c.m. cosine)	235 MeV/c	245 MeV/c	255 MeV/c	265 MeV/c	
−0.875	1.22±0.61	1.75±0.53	0.66±0.23	1.05±0.24	
−0.625	1.06±0.47	0.83±0.32	0.79±0.24	0.38±0.12	
−0.375	1.07±0.48	0.72±0.27	0.76±0.21	1.07±0.23	
−0.125	1.36±0.51	1.09±0.35	0.77±0.20	0.83±0.17	
0.125	0.58±0.34	1.34±0.36	0.71±0.19	0.75±0.16	
0.375	1.06±0.43	1.09±0.31	0.97±0.22	0.65±0.15	
0.625	0.54±0.31	0.44±0.20	0.45±0.15	0.38±0.11	
0.875	0.66±0.33	0.61±0.23	0.73±0.18	0.57±0.13	
Center of bin (c.m. cosine)	275 MeV/c	285 MeV/c	295 MeV/c	305 MeV/c	
−0.875	1.47±0.26	0.69±0.15	0.93±0.18	1.06±0.20	
−0.625	1.18±0.22	0.57±0.14	0.94±0.17	0.69±0.15	
−0.375	0.79±0.17	0.75±0.15	0.66±0.15	0.65±0.14	
−0.125	0.78±0.15	0.56±0.11	0.57±0.12	0.84±0.15	
0.125	0.63±0.13	0.54±0.11	0.68±0.13	0.34±0.09	
0.375	0.58±0.13	0.54±0.11	0.63±0.12	0.43±0.10	
0.625	0.54±0.12	0.41±0.09	0.33±0.09	0.32±0.09	
0.875	0.42±0.11	0.31±0.08	0.14±0.06	0.36±0.09	
Center of bin (c.m. cosine)	315 MeV/c	325 MeV/c	335 MeV/c	345 MeV/c	355 MeV/c
−0.950	0.84±0.27	1.01±0.25	0.61±0.19	0.44±0.17	0.67±0.12
−0.850	0.71±0.24	0.53±0.18	0.91±0.22	0.80±0.22	0.51±0.11
−0.750	0.56±0.20	0.84±0.26	0.76±0.20	0.54±0.18	0.60±0.14
−0.650	0.83±0.24	1.08±0.28	0.68±0.18	0.33±0.13	0.82±0.14
−0.550	0.73±0.22	1.29±0.43	0.71±0.19	0.58±0.20	0.79±0.13
−0.450	0.92±0.29	0.67±0.28	0.82±0.23	0.74±0.24	0.61±0.11
−0.350	0.34±0.15	0.65±0.19	0.58±0.16	0.68±0.18	0.67±0.12
−0.250	0.51±0.18	0.67±0.19	0.92±0.20	0.60±0.17	0.60±0.11
−0.150	0.54±0.18	0.64±0.17	0.49±0.14	0.86±0.20	0.49±0.09
−0.050	0.88±0.22	0.79±0.19	0.73±0.17	0.62±0.16	0.51±0.10
0.050	0.38±0.15	0.98±0.21	0.42±0.13	0.68±0.17	0.68±0.11
0.150	0.50±0.17	0.58±0.16	0.31±0.11	0.29±0.11	0.52±0.09
0.250	0.53±0.17	0.56±0.16	0.49±0.14	0.50±0.14	0.42±0.08
0.350	0.21±0.10	0.61±0.16	0.38±0.12	0.29±0.11	0.46±0.09
0.450	0.37±0.14	0.38±0.13	0.67±0.16	0.41±0.13	0.25±0.06
0.550	0.46±0.15	0.17±0.08	0.45±0.13	0.28±0.10	0.36±0.07
0.650	0.31±0.13	0.41±0.13	0.44±0.13	0.51±0.14	0.39±0.08
0.750	0.46±0.15	0.16±0.08	0.40±0.12	0.51±0.14	0.54±0.09
0.850	0.35±0.13	0.44±0.13	0.43±0.13	0.54±0.14	0.89±0.12
0.950	0.40±0.14	0.57±0.15	0.61±0.15	0.51±0.14	0.72±0.10
Center of bin (c.m. cosine)	365 MeV/c	375 MeV/c	385 MeV/c	395 MeV/c	405 MeV/c
−0.950	0.83±0.09	1.27±0.09	2.30±0.11	2.97±0.14	2.84±0.15
−0.850	0.76±0.08	1.23±0.09	1.95±0.10	2.33±0.12	2.25±0.13
−0.750	0.79±0.09	1.13±0.08	1.54±0.09	1.80±0.11	1.63±0.11
−0.650	0.62±0.08	0.92±0.08	1.09±0.07	1.28±0.10	1.19±0.10
−0.550	0.72±0.09	0.88±0.08	0.87±0.06	0.83±0.07	0.68±0.07
−0.450	0.57±0.07	0.86±0.08	0.81±0.07	0.52±0.06	0.40±0.05
−0.350	0.52±0.06	0.56±0.06	0.57±0.05	0.36±0.04	0.24±0.04
−0.250	0.48±0.06	0.60±0.06	0.42±0.04	0.20±0.03	0.15±0.03
−0.150	0.53±0.06	0.49±0.05	0.29±0.03	0.09±0.02	0.02±0.01
−0.050	0.45±0.06	0.33±0.04	0.23±0.03	0.02±0.01	0.01±0.01
0.050	0.45±0.06	0.31±0.04	0.17±0.02	0.05±0.01	0.05±0.01
0.150	0.34±0.05	0.38±0.04	0.17±0.02	0.07±0.02	0.11±0.02
0.250	0.39±0.05	0.39±0.04	0.37±0.04	0.22±0.03	0.17±0.03

TABLE I. *(Continued)*

Center of bin (c.m. Cosine)	365 MeV/c	375 MeV/c	385 MeV/c	395 MeV/c	405 MeV/c
0.350	0.48± 0.06	0.49± 0.05	0.52±0.04	0.40 ± 0.04	0.33± 0.04
0.450	0.48± 0.06	0.52± 0.05	0.68±0.05	0.60 ± 0.05	0.56± 0.05
0.550	0.51± 0.06	0.78± 0.06	0.93±0.06	0.96 ± 0.06	0.71± 0.06
0.650	0.51± 0.06	0.85± 0.06	1.30±0.07	1.16 ± 0.07	1.01± 0.07
0.750	0.75± 0.07	1.26± 0.07	1.71±0.08	1.57 ± 0.08	1.20± 0.08
0.850	0.94± 0.08	1.64± 0.08	2.10±0.08	1.99 ± 0.09	1.47± 0.09
0.950	1.22± 0.09	1.94± 0.09	2.76±0.10	2.54 ± 0.10	1.75± 0.10
Center of bin (c.m. cosine)	415 MeV/c	425 MeV/c	435 MeV/c	445 MeV/c	455 MeV/c
−0.950	2.67± 0.19	2.07 ± 0.29	1.93 ± 0.31	1.83± 0.32	1.41 ± 0.42
−0.850	1.72± 0.15	1.66 ± 0.24	1.55 ± 0.27	1.00± 0.24	0.69 ± 0.28
−0.750	1.15± 0.12	1.05 ± 0.21	0.76 ± 0.19	0.58± 0.18	0.74 ± 0.28
−0.650	0.92± 0.11	0.61 ± 0.15	0.48 ± 0.14	0.46± 0.16	0.10 ± 0.10
−0.550	0.42± 0.07	0.42 ± 0.11	0.50 ± 0.14	0.42 ± 0.15	0.00 ± 0.00
−0.450	0.34± 0.06	0.17 ± 0.07	0.27 ± 0.10	0.19 ± 0.09	0.21 ± 0.15
−0.350	0.17± 0.04	0.31 ± 0.09	0.21 ± 0.10	0.24 ± 0.11	0.93 ± 0.31
−0.250	0.13± 0.04	0.16 ± 0.07	0.30 ± 0.11	0.19 ± 0.10	0.00 ± 0.00
−0.150	0.07± 0.03	0.21 ± 0.07	0.16 ± 0.08	0.19 ± 0.10	0.09 ± 0.09
−0.050	0.04± 0.02	0.05 ± 0.04	0.11 ± 0.06	0.10 ± 0.07	0.09 ± 0.09
0.050	0.07± 0.03	0.10 ± 0.05	0.11 ± 0.06	0.42 ± 0.14	0.00 ± 0.00
0.150	0.15± 0.04	0.10 ± 0.05	0.18 ± 0.08	0.14 ± 0.08	0.09 ± 0.09
0.250	0.25± 0.05	0.34 ± 0.09	0.28 ± 0.10	0.14 ± 0.08	0.18 ± 0.13
0.350	0.37± 0.06	0.32 ± 0.09	0.35± 0.11	0.40 ± 0.13	0.27 ± 0.15
0.450	0.37± 0.06	0.51 ± 0.11	0.31 ± 0.10	0.31 ± 0.12	0.70 ± 0.25
0.550	0.59± 0.07	0.35 ± 0.09	0.51 ± 0.13	0.22 ± 0.10	0.34 ± 0.17
0.650	0.78± 0.08	0.57 ± 0.11	0.44 ± 0.12	0.35 ± 0.12	0.26 ± 0.15
0.750	0.80± 0.08	0.59 ± 0.11	0.56 ± 0.14	0.82 ± 0.20	0.19 ± 0.14
0.850	1.01± 0.09	0.93 ± 0.14	0.89 ± 0.17	0.48 ± 0.14	0.51 ± 0.21
0.950	1.16± 0.10	1.32 ± 0.17	0.96 ± 0.18	0.70 ± 0.17	0.94 ± 0.28

TABLE II. Legendre-polynomial coefficients A_l/A_0 for $K^-p \to \bar{K}^0 n$.

Momentum (MeV/c)	A_1/A_0	A_2/A_0	A_3/A_0	A_4/A_0
235	−0.37 ± 0.28			
245	−0.36 ± 0.20			
255	−0.05 ± 0.18			
265	−0.32 ± 0.14			
275	−0.60 ± 0.10			
285	−0.38 ± 0.13			
295	−0.70 ± 0.11			
305	−0.64 ± 0.11			
315	−0.38 ± 0.13	0.02 ± 0.18	0.20 ± 0.22	−0.01± 0.23
325	−0.52 ± 0.11	−0.09 ± 0.15	0.36± 0.18	0.28± 0.19
335	−0.32 ± 0.11	0.09 ± 0.14	0.25± 0.16	−0.02± 0.18
345	−0.17 ± 0.12	−0.03 ± 0.15	0.41 ± 0.18	0.09± 0.21
355	−0.12 ± 0.08	0.23 ± 0.09	0.46 ± 0.11	0.15± 0.13
365	0.04 ± 0.05	0.67 ± 0.06	0.32 ± 0.07	0.11 ± 0.08
375	0.13 ± 0.04	1.11 ± 0.04	0.39 ± 0.05	−0.04 ± 0.06
385	0.11 ± 0.03	1.65 ± 0.03	0.17 ± 0.04	0.03 ± 0.04
395	−0.13 ± 0.04	2.00 ± 0.03	−0.15 ± 0.04	0.07 ± 0.05
405	−0.35 ± 0.04	2.03 ± 0.04	−0.45 ± 0.05	0.09 ± 0.05
415	−0.49 ± 0.06	1.94 ± 0.05	−0.69 ± 0.07	0.20 ± 0.08
425	−0.39 ± 0.11	1.84 ± 0.10	−0.49 ± 0.13	0.40 ± 0.16
435	−0.43 ± 0.13	1.66 ± 0.13	−0.52 ± 0.16	0.35 ± 0.19
445	−0.43 ± 0.15	1.47 ± 0.17	−0.58 ± 0.20	0.54 ± 0.23
455	−0.25 ± 0.25	1.41 ± 0.25	−0.33 ± 0.29	0.28 ± 0.42

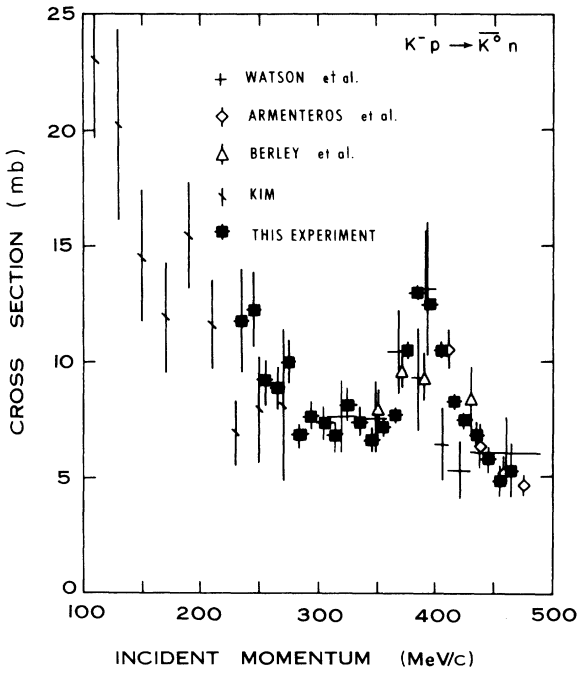

FIG. 6. Cross section (mb) for the charge-exchange reaction $K^-p \rightarrow \bar{K}^0 n$ as a function of incident momentum (MeV/c). The data of Watson *et al.* (Ref. 3), Armenteros *et al.* (Ref. 10), Berley *et al.* (Ref. 7), and Kim (Ref. 12) are shown for comparison.

TABLE III. Total partial cross sections for $K^-p \rightarrow K^-p$, $K^-p \rightarrow \bar{K}^0 n$, and $K^-p \rightarrow$all.

Momentum (MeV/c)	$K^-p \rightarrow K^-p$ (mb)	$K^-p \rightarrow \bar{K}^0 n$ (mb)	$K^-p \rightarrow$all (mb)
225	65.41 ± 10.30	16.84 ± 4.72	•••
235	55.74 ± 5.34	11.75 ± 2.26	•••
245	53.24 ± 3.76	12.25 ± 1.67	113.8 ± 8.0
255	49.22 ± 2.70	9.11 ± 1.01	98.0 ± 5.3
265	47.71 ± 2.27	8.85 ± 0.85	94.0 ± 4.4
275	48.75 ± 2.20	9.97 ± 0.86	96.7 ± 4.2
285	39.42 ± 1.63	6.79 ± 0.59	75.1 ± 3.0
295	41.22 ± 1.86	7.60 ± 0.66	82.5 ± 3.5
305	40.36 ± 2.02	7.32 ± 0.65	78.6 ± 3.5
315	37.02 ± 1.93	6.73 ± 0.59	70.9 ± 3.2
325	40.28 ± 2.06	8.13 ± 0.65	76.0 ± 3.1
335	37.84 ± 1.83	7.35 ± 0.53	71.5 ± 2.8
345	37.26 ± 1.95	6.67 ± 0.52	71.3 ± 2.9
355	34.77 ± 1.79	7.16 ± 0.34	68.8 ± 2.3
365	34.21 ± 1.71	7.69 ± 0.24	70.0 ± 2.0
375	36.67 ± 1.83	10.49 ± 0.25	81.8 ± 2.1
385	33.89 ± 1.37	12.95 ± 0.25	88.3 ± 1.7
395	38.47 ± 1.57	12.45 ± 0.27	91.6 ± 1.9
405	32.06 ± 1.39	10.45 ± 0.28	76.6 ± 1.7
415	32.59 ± 1.67	8.21 ± 0.29	70.7 ± 2.0
425	31.19 ± 1.97	7.37 ± 0.38	66.7 ± 2.6
435	26.83 ± 1.79	6.77 ± 0.46	54.9 ± 2.5
445	28.83 ± 2.21	5.72 ± 0.50	55.7 ± 3.0
455	30.32 ± 3.16	4.83 ± 0.58	57.2 ± 4.2
465	31.99 ± 5.92	5.24 ± 1.15	•••

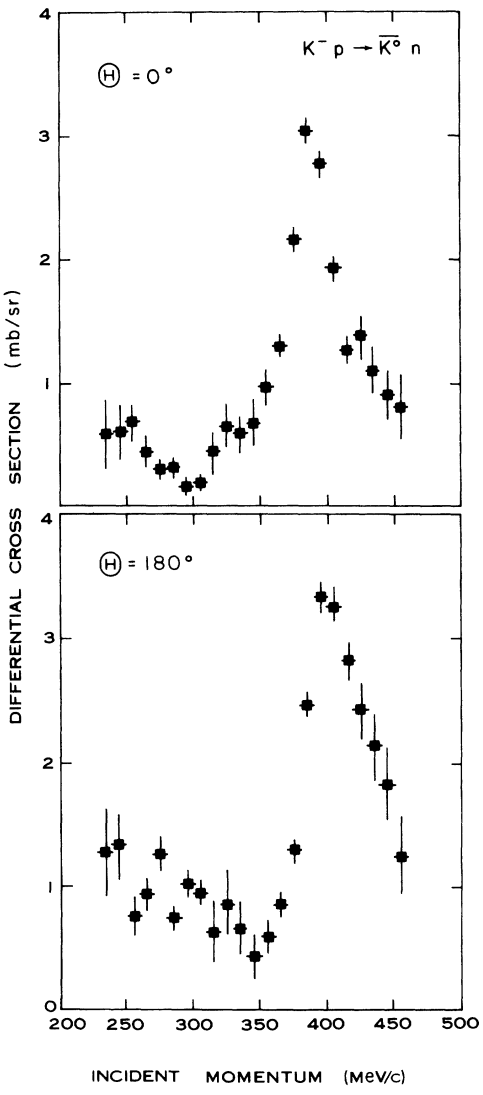

FIG. 7. Differential cross sections (mb/sr) at 0° and 180° for the reaction $K^-p \rightarrow \bar{K}^0 n$ for events binned in intervals of 10 MeV/c incident K^- momentum.

Of those events fitting two hypotheses, 91% have the K^-p elastic hypothesis as one of two. Most of the ambiguities are with the $\Sigma^+\pi^-$ final state where the Σ^+ is zero length, the π^-p final state, and the π^-p, π^0 final state. On the basis of confidence levels and measured ionization information, all but 1% were accepted as K^-p elastic events. The remaining 1% were π^-p elastic scatterings. A small number of events where the scattered K^- decayed or elastically scattered again were described by the scanners as charged-Σ production and decay. A negligible number of these events

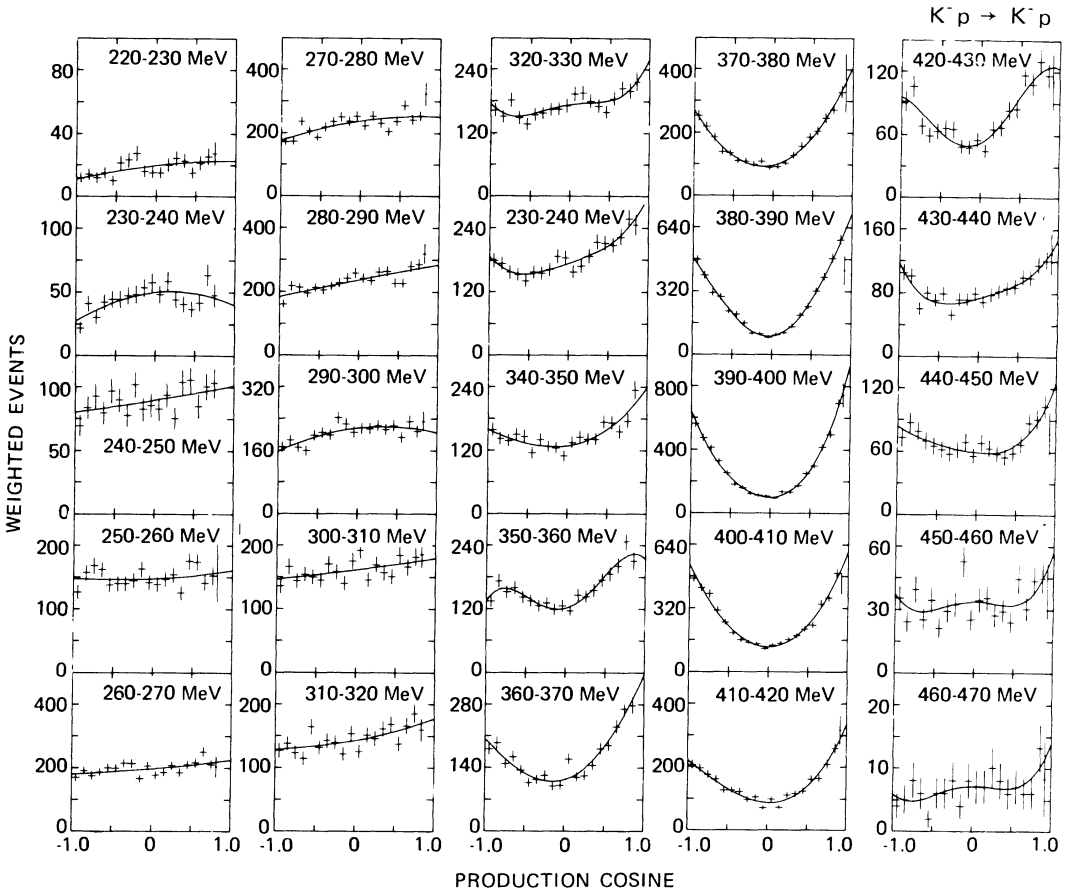

FIG. 8. The production-cosine distributions for the reaction $K^-p \to K^-p$ for events binned in intervals of 10 MeV/c incident K^- momentum. The curves are from the fits to Legendre polynomials described in the text.

satisfied the cuts for elastic scatterings.

The above separation of hypotheses yielded a sample of 64 600 K^-p elastic scatterings. This sample of events showed a loss of events with short proton tracks in a plane seen edge-on by the scanner. The azimuthal distribution of the scattered proton about the beam was used to measure this loss. The distribution was divided into up-down and left-right events, and, assuming 100% detection efficiency for the left-right events, a weight was established as a function of proton laboratory momentum. The mean weight was 1.07. The distribution of errors in the fitted incident K^- momentum is shown in Fig. 3(a).

C. Cross sections

The cross sections for these reactions were determined from a path length based on the τ decays of the beam. The analysis of these τ's has been described in a previous publication.[4] The numbers of both τ's and $\overline{K}^0$'s were both corrected by factors of 18.0 and 2.88, respectively, for unobserved decay modes using the known branching fractions.[5] All events have been corrected for measuring losses and scanning losses.

The scanning efficiencies were determined from the multiple scans by using an extension of the method developed by Derenzo and Hildebrand.[6] The analysis accounts for the differing visibility of events by parameterizing a visibility function $f(v)$; $f(v)$ is the fraction of the sample seen with an efficiency v, where v varies from 0.0 to 1.0. The extension used for this experiment defines a different visibility (v_1, v_2, and v_3) for each of the three scans. The events found on each of the scans are fitted to determine the parameters of the function $f(v_1, v_2, v_3)$ which is then used to calculate the efficiencies after one, two, and three scans. Details of this analysis can be found in Ref. 6.

Those events satisfying the cuts described above

and in regions of high visibility were used to determine the scan efficiencies. The overall efficiencies were 0.92 and 0.98 for charge-exchange and elastic events, respectively.

Additional losses were due to measurement failures. For each reaction these were divided into two groups. The first group included events which failed for reasons independent of their configuration, such as bookkeeping errors or obscuration of the vertex by flares or overlapping beam tracks. Most of the events were in this group, and we assumed that these events had the same configuration and passing rate as those events which were successfully measured and fitted. To account for losses of this nature the measured events were increased by 1.095 and 1.042 for the charge-exchange and elastic events, respectively. A second group of events were measured and failed to fit a reaction hypothesis for reasons which could depend on the track configuration, such as short tracks. The raw measurement information was used to check whether these events passed the cuts applied to the passing events. To account for losses of this type the measured events were weighted by 1.009 and 1.012 for the charge-exchange and elastic events, respectively.

Finally, the fits to the angular distributions (described below) of the K^-p elastic were used to calculate the fraction at each momentum of the K^-p events which had been removed by the cut on scattered-proton momentum. These fractions were used to correct the elastic cross sections for this cut.

Comparison of the cross sections of events from different beam settings disclosed a systematic error which had been introduced by beam averaging of the individual events in SQUAW. For each of the 24 beam settings an average beam momentum was determined from the τ's, and for each event this beam momentum was averaged with the measured momentum of the K^- track before kinematic fittings. This beam-averaging procedure was applied to all events, including the τ's which were used to determine the path length. In general, the track momentum resolutions differ for each topology, and consequently the ability of the fit to constrain the K^- incident momentum varies with topology. The beam-averaging procedure then affected the K^- momentum measurement differently for different topologies. As a result the momentum distributions of the events were distorted, and the cross sections from events in the centers of a momentum distribution differed from those based on events at the edges of a distribution. The experiment of Berley *et al.*,[7] which measured the charge-exchange reaction in this momentum region, also found cross sections and coefficients from different runs to be inconsistent (see Figs. 5 and 6). Using the known beam-averaging procedure and the known error distributions, we derived an algorithm for correcting the cross sec-

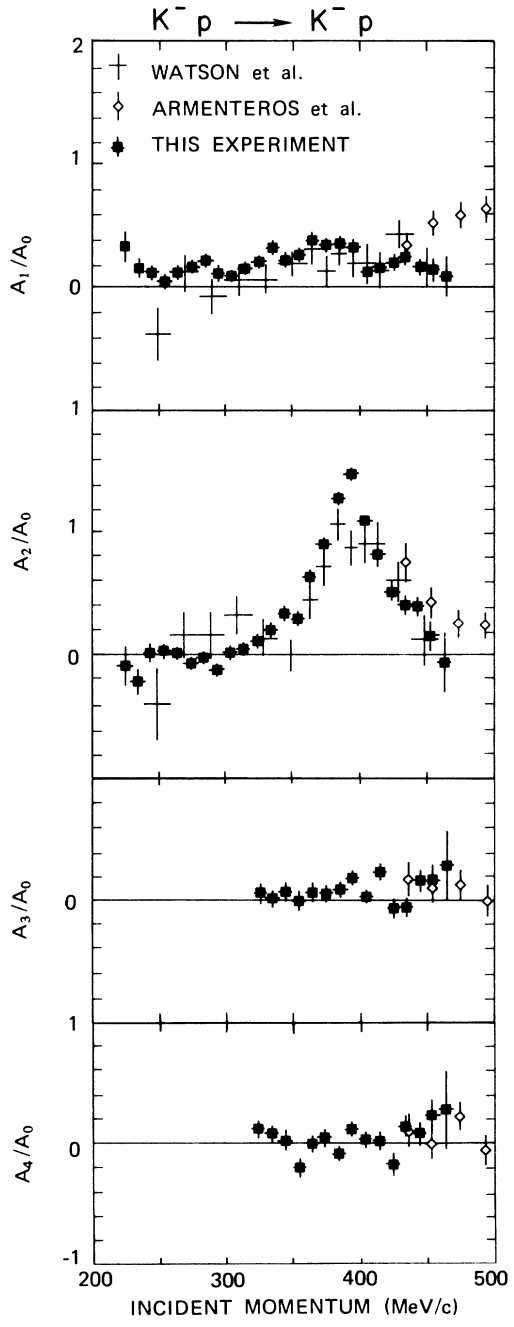

FIG. 9. Legendre coefficients A_l/A_0 ($l=1,4$) as a function of incident momentum for the angular distribution in the reaction $K^-p \to K^-p$. The data of Watson *et al.* (Ref. 3) and Armenteros *et al.* (Ref. 10) are shown for comparison.

TABLE IV. Differential cross section for the reaction $K^-p \to K^-p$ (mb/sr). The last entry for each momentum is the cut on the c.m. cosine.

Center of bin (c.m. cosine)	225 MeV/*c*	235 MeV/*c*	245 MeV/*c*	255 MeV/*c*	265 MeV/*c*
−0.95	3.16±0.91	2.22±0.47	3.32±0.40	3.16±0.28	3.07±0.24
−0.85	3.70±0.99	4.10±0.64	3.98±0.44	3.92±0.31	3.48±0.25
−0.75	3.18±0.92	2.98±0.54	4.40±0.46	4.19±0.32	3.20±0.24
−0.65	3.98±1.03	4.16±0.64	3.77±0.42	4.04±0.32	3.40±0.25
−0.55	2.66±0.84	4.34±0.65	4.57±0.47	3.44±0.29	3.67±0.26
−0.45	5.59±1.22	4.33±0.65	4.23±0.45	3.49±0.30	3.63±0.26
−0.35	6.14±1.28	4.62±0.67	3.65±0.42	3.48±0.30	3.93±0.27
−0.25	7.22±1.39	4.72±0.68	4.78±0.48	3.61±0.30	3.92±0.27
−0.15	4.29±1.07	5.21±0.72	3.88±0.43	4.06±0.32	3.05±0.24
−0.05	4.03±1.04	5.60±0.74	4.02±0.44	3.53±0.30	3.77±0.26
0.05	4.03±1.04	4.72±0.68	3.88±0.43	3.46±0.29	3.26±0.24
0.15	5.39±1.21	5.71±0.75	4.40±0.46	3.66±0.30	3.41±0.25
0.25	6.49±1.32	4.34±0.65	3.55±0.41	3.83±0.31	3.81±0.26
0.35	6.10±1.30	4.00±0.63	4.89±0.48	3.13±0.28	3.41±0.25
0.45	4.04±1.08	3.63±0.61	4.97±0.49	4.37±0.33	3.88±0.27
0.55	5.72±1.31	4.11±0.67	4.01±0.45	4.34±0.34	3.98±0.28
0.65	6.85±1.50	6.31±0.85	4.74±0.50	3.52±0.31	4.59±0.30
0.75	7.39±2.05	4.75±0.90	4.89±0.55	3.81±0.35	3.87±0.29
0.85				3.99±1.20	3.74±0.62
Cut	0.77	0.78	0.80	0.81	0.82

Center of bin (c.m. cosine)	275 MeV/*c*	285 MeV/*c*	295 MeV/*c*	305 MeV/*c*	315 MeV/*c*
−0.95	2.75±0.21	2.01±0.16	2.62±0.20	2.69±0.23	2.58±0.23
−0.85	2.77±0.21	2.73±0.19	2.88±0.21	3.27±0.25	2.78±0.24
−0.75	3.77±0.25	2.69±0.18	2.60±0.20	2.83±0.24	2.49±0.22
−0.65	3.30±0.23	2.47±0.18	2.48±0.20	3.01±0.24	2.30±0.22
−0.55	2.98±0.22	2.71±0.19	3.08±0.22	2.92±0.24	3.28±0.26
−0.45	3.50±0.24	2.62±0.18	3.19±0.22	2.82±0.24	2.63±0.23
−0.35	3.78±0.25	2.76±0.19	3.10±0.22	3.30±0.25	2.84±0.24
−0.25	4.02±0.25	2.91±0.19	3.78±0.24	3.06±0.24	2.78±0.24
−0.15	3.81±0.25	3.10±0.20	3.55±0.24	2.71±0.23	2.41±0.22
−0.05	4.07±0.26	3.32±0.21	3.22±0.22	3.39±0.26	3.05±0.25
0.05	3.57±0.24	3.12±0.20	3.39±0.23	3.72±0.27	2.49±0.22
0.15	4.07±0.26	3.02±0.20	3.36±0.23	2.82±0.23	3.00±0.24
0.25	3.71±0.24	3.36±0.21	3.49±0.23	3.27±0.25	2.88±0.24
0.35	3.29±0.23	3.39±0.21	3.33±0.23	3.04±0.24	3.18±0.25
0.45	3.81±0.25	2.91±0.19	3.48±0.23	2.93±0.24	3.32±0.26
0.55	4.61±0.28	2.91±0.19	3.03±0.22	3.59±0.27	2.73±0.23
0.65	3.88±0.26	3.57±0.22	3.65±0.25	3.23±0.26	3.28±0.26
0.75	4.08±0.28	3.64±0.23	3.25±0.24	3.54±0.28	3.66±0.29
0.85	5.18±0.62	4.05±0.42	3.64±0.39	3.62±0.40	3.16±0.35
Cut	0.83	0.84	0.85	0.86	0.87

Center of bin (c.m. cosine)	325 MeV/*c*	335 MeV/*c*	345 MeV/*c*	355 MeV/*c*	365 MeV/*c*
−0.95	2.85±0.23	2.68±0.20	3.12±0.25	2.27±0.20	2.90±0.22
−0.85	2.65±0.22	2.61±0.20	2.78±0.24	2.92±0.23	3.11±0.23
−0.75	3.21±0.24	2.38±0.19	2.70±0.23	2.59±0.21	2.38±0.20
−0.65	2.64±0.22	2.33±0.19	2.94±0.24	2.75±0.22	2.64±0.21
−0.55	2.42±0.21	2.16±0.18	2.86±0.24	2.46±0.21	2.17±0.19
−0.45	2.75±0.22	2.45±0.20	2.25±0.21	2.34±0.20	1.73±0.17
−0.35	2.81±0.23	2.41±0.20	2.73±0.23	2.19±0.20	1.85±0.18
−0.25	2.94±0.23	2.54±0.20	2.46±0.22	2.29±0.20	2.00±0.18
−0.15	2.96±0.23	2.95±0.22	2.41±0.22	2.08±0.19	1.62±0.16
−0.05	3.06±0.24	2.91±0.22	2.11±0.20	2.21±0.20	1.65±0.17

TABLE IV. *(continued)*

Center of bin (c.m. cosine)	325 MeV/c	335 MeV/c	345 MeV/c	355 MeV/c	365 MeV/c
0.05	3.51±0.25	2.51±0.20	2.60±0.23	2.05±0.19	2.60±0.21
0.15	3.50±0.25	2.68±0.21	2.79±0.23	2.57±0.21	1.93±0.18
0.25	3.24±0.24	2.98±0.22	2.68±0.23	2.51±0.21	2.00±0.18
0.35	3.04±0.24	3.40±0.24	2.68±0.23	2.72±0.22	2.36±0.20
0.45	2.86±0.23	3.36±0.23	3.32±0.25	3.06±0.23	2.95±0.22
0.55	3.33±0.25	3.29±0.23	3.29±0.25	3.24±0.24	3.06±0.22
0.65	3.72±0.26	3.52±0.24	2.98±0.24	3.50±0.25	3.70±0.25
0.75	3.59±0.27	4.05±0.27	3.37±0.27	4.28±0.29	4.35±0.28
0.85	3.96±0.36	3.95±0.32	4.63±0.36	3.69±0.30	4.53±0.31
Cut	0.88	0.88	0.89	0.89	0.90
Center of bin (c.m. cosine)	375 MeV/c	385 MeV/c	395 MeV/c	405 MeV/c	415 MeV/c
−0.95	3.80±0.24	4.30±0.20	5.01±0.21	4.06±0.19	3.27±0.23
−0.85	3.30±0.22	3.58±0.18	4.19±0.19	3.63±0.18	3.13±0.23
−0.75	2.79±0.21	2.79±0.16	3.61±0.18	3.36±0.17	2.86±0.22
−0.65	2.13±0.18	2.59±0.15	2.87±0.16	2.63±0.15	2.64±0.21
−0.55	2.05±0.18	1.93±0.13	2.19±0.14	2.11±0.13	2.09±0.19
−0.45	1.73±0.16	1.79±0.13	1.56±0.12	1.65±0.12	2.10±0.19
−0.35	1.70±0.16	1.40±0.11	1.35±0.11	1.36±0.11	2.02±0.18
−0.25	1.53±0.16	0.95±0.09	1.06±0.09	1.27±0.10	1.60±0.16
−0.15	1.69±0.16	0.91±0.09	0.93±0.09	1.21±0.10	1.74±0.17
−0.05	1.38±0.15	0.77±0.08	0.89±0.09	1.02±0.09	1.16±0.14
0.05	1.39±0.15	0.90±0.09	0.80±0.08	1.19±0.10	1.58±0.16
0.15	1.55±0.15	1.00±0.09	1.15±0.10	1.30±0.11	1.15±0.14
0.25	1.89±0.17	1.29±0.11	1.16±0.10	1.49±0.12	1.73±0.16
0.35	2.28±0.18	1.78±0.13	1.54±0.12	1.68±0.12	1.78±0.17
0.45	2.66±0.20	2.21±0.14	2.20±0.14	1.97±0.13	1.87±0.17
0.55	2.94±0.21	2.91±0.16	2.66±0.15	2.15±0.14	2.44±0.19
0.65	3.52±0.23	3.54±0.18	3.68±0.18	3.07±0.17	2.49±0.20
0.75	3.92±0.25	4.4 ±0.21	4.41±0.20	3.33±0.18	3.17±0.22
0.85	4.87±0.30	5.31±0.24	6.23±0.26	4.44±0.22	3.96±0.27
0.91	5.58±1.44	4.09±0.71	7.01±0.76	4.15±0.51	5.11±0.74
Cut	0.91	0.91	0.91	0.92	0.92
Center of bin (c.m. cosine)	425 MeV/c	435 MeV/c	445 MeV/c	455 MeV/c	465 MeV/c
−0.95	2.75±0.29	2.43±0.24	2.20±0.26	2.40±0.41	1.46±0.73
−0.85	3.26±0.32	2.32±0.23	2.62±0.28	1.67±0.34	2.00±0.89
−0.75	2.14±0.26	1.38±0.18	2.37±0.27	2.74±0.44	3.40±1.20
−0.65	1.89±0.25	1.81±0.20	2.10±0.25	1.77±0.35	2.63±1.07
−0.55	2.04±0.26	1.61±0.19	1.95±0.24	2.42±0.41	0.88±0.62
−0.45	2.15±0.27	1.79±0.20	1.86±0.24	1.49±0.33	2.61±1.06
−0.35	2.11±0.26	1.20±0.17	1.75±0.23	2.06±0.38	2.56±1.04
−0.25	1.56±0.23	1.64±0.19	1.88±0.24	2.27±0.40	3.33±1.18
−0.15	1.49±0.22	1.65±0.20	2.10±0.26	3.67±0.51	1.62±0.81
−0.05	1.66±0.23	1.82±0.21	1.71±0.23	1.76±0.35	3.14±1.11
0.05	1.31±0.20	1.59±0.19	2.10±0.26	2.37±0.41	2.66±1.01
0.15	1.86±0.23	1.81±0.21	1.95±0.25	2.43±0.41	2.56±0.97
0.25	1.88±0.23	1.91±0.21	1.80±0.24	1.86±0.36	3.50±1.11
0.35	2.30±0.25	2.01±0.22	1.72±0.23	1.98±0.37	2.66±0.94
0.45	2.31±0.25	2.04±0.22	1.85±0.24	1.63±0.33	1.89±0.77
0.55	3.20±0.30	2.35±0.24	2.10±0.26	2.96±0.45	2.08±0.79
0.65	2.95±0.29	2.33±0.24	2.74±0.30	2.00±0.37	1.70±0.69
0.75	3.57±0.32	2.71±0.25	2.84±0.30	2.86±0.44	1.66±0.68
0.85	3.24±0.32	2.84±0.28	3.21±0.34	2.95±0.47	3.61±1.04
0.91	3.22±0.78	3.16±0.63	2.51±0.65	2.64±0.88	2.36±1.67
Cut	0.92	0.93	0.93	0.93	0.93

TABLE V. Legendre-polynomial coefficients A/A_0 for $K^-p \to K^-p$.

Momentum (MeV/c)	A_1/A_0	A_2/A_0	A_3/A_0	A_4/A_0
225	0.32±0.12	−0.10±0.16		
235	0.14±0.08	−0.22±0.10		
245	0.11±0.05	0.02±0.07		
255	0.04±0.04	0.03±0.06		
265	0.12±0.03	0.01±0.05		
275	0.16±0.03	−0.07±0.04		
285	0.22±0.03	−0.03±0.04		
295	0.11±0.03	−0.12±0.04		
305	0.10±0.04	0.02±0.05		
315	0.15±0.04	0.05±0.15		
325	0.21±0.04	0.12±0.06	0.06±0.07	0.12±0.07
335	0.33±0.04	0.20±0.06	0.02±0.07	0.08±0.07
345	0.22±0.04	0.33±0.06	0.07±0.07	0.02±0.07
355	0.27±0.04	0.30±0.06	−0.00±0.07	−0.20±0.07
365	0.39±0.04	0.64±0.06	0.06±0.07	−0.01±0.07
375	0.35±0.04	0.90±0.05	0.06±0.06	0.04±0.07
385	0.35±0.04	1.28±0.04	0.09±0.05	−0.09±0.05
395	0.33±0.03	1.47±0.04	0.17±0.04	0.11±0.05
405	0.14±0.03	1.09±0.04	0.03±0.05	0.03±0.05
415	0.15±0.04	0.82±0.05	0.23±0.06	0.01±0.07
425	0.21±0.06	0.53±0.08	−0.07±0.09	−0.18±0.10
435	0.26±0.05	0.41±0.07	−0.06±0.08	0.13±0.09
445	0.17±0.06	0.40±0.08	0.15±0.09	0.07±0.10
455	0.15±0.08	0.16±0.11	0.15±0.13	0.23±0.13
465	0.10±0.17	0.06±0.24	0.28±0.28	0.27±0.30

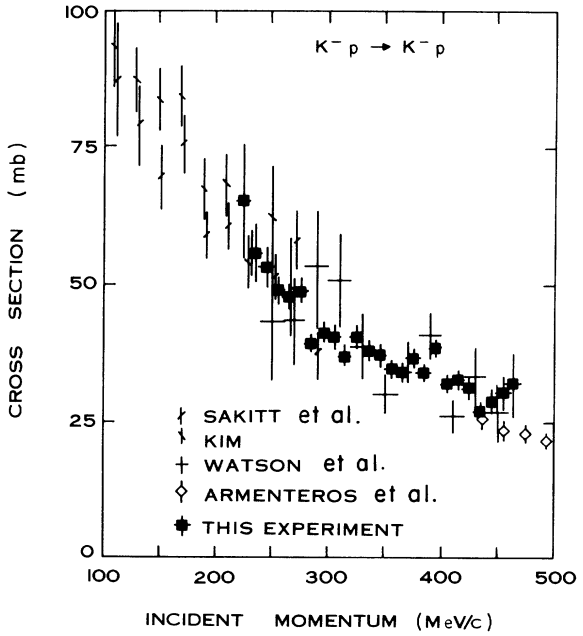

FIG. 10. Cross section (mb) for the elastic scattering $K^-p \to K^-p$ as a function of incident momentum (MeV/c). The data of Sakitt *et al.* (Ref. 11), Watson *et al.* (Ref. 3), and Armenteros *et al.* (Ref. 10) are shown for comparison.

tions and Legendre coefficients.[8] The algorithm also included an unfolding of the uncertainty in the beam momentum. The algorithm was applied to the data, and the resulting cross sections from different beam settings agreed well. The changes in the final cross sections and coefficients averaged much less than a standard deviation. A few points were changed by as much as 1.5 standard deviations. All the results described in the following section have been corrected.

III. RESULTS

A. Charge exchange

The events were binned in intervals of 10 MeV/c incident momentum, and the angular distribution for each interval is shown in Fig. 4. The curves are from fits described below. The differential cross sections are listed in Table I. Below 310 MeV/c the distributions are consistent with being linear in $\cos\theta$. In the region near 390 MeV/c the distribution becomes strongly peaked backward and forward, showing the $\cos^2\theta$ dependence from

the resonant D wave [$\Lambda(1520), \frac{3}{2}^-$] and its interference with a large S-wave background. As the momentum increases through the resonance region the cross section is first peaked more forward and then becomes peaked more backward as the resonant D wave interferes first constructively and then destructively with small background P waves.

The maximum-likelihood technique was used to fit each distribution to a Legendre polynomial expansion. The resulting fits are plotted as curves over the data in Fig. 4. The Legendre coefficients are listed in Table II and plotted as a function of incident momentum in Fig. 5.[9] Also shown are the data of Berley *et al.*[7] and Armenteros *et al.*[10] Below 310 MeV/c the expansion included only A_1/A_0.

The dominant structure is seen in the A_2/A_0 coefficient, which rises dramatically near 390 MeV/c. The data of Berley fall significantly below ours near the resonance. Their data are also internally inconsistent at 390 MeV/c, where they had two overlapping runs. At the highest energies we match smoothly with the data of Armenteros. The A_1/A_0 coefficients show structure in the resonance region from the interference between the D wave and background P waves. Again we smoothly join the data of Armenteros and fall somewhat below the points of Berley. Above 390 MeV/c we find significant A_4/A_0, indicating the onset of some D_5 contribution. Other than the structure seen from the resonant D wave and its interference with slowly varying background we see no significant structure.

The charge-exchange cross section is shown in Fig. 6 and listed in Table III. The data of Watson *et al.*,[3] Armenteros *et al.*,[10] Berley *et al.*,[7] and Kim[10] are shown for comparison. We join smoothly to the high-statistics data of Armenteros at the high-energy end, and in general we find agreement with the other experiments. The enhancement from the $\Lambda(1520)$ is about 7 mb, and this implies an elasticity of the resonance of about 0.42, in agreement with the present world summary value 0.45 ± 0.01. A more accurate estimate of the elasticity from these data will emerge from a full partial-wave analysis of this and the other channels.

The differential cross sections at 0° and 180° have been calculated from the Legendre coefficients and the total cross sections. These are displayed as a function of incident momentum in Fig. 7. Uncertainties are calculated using the full error matrix.

B. K^-p final state

The data have been divided into intervals of 10 MeV/c incident momentum, and the angular distribution for each interval is shown in Fig. 8. The differential cross sections are listed in Table IV. As in the charge-exchange channel the major structure occurs in the region of the $\Lambda(1520)$, where the resonant D wave interferes with the dominant S-wave background.

The distributions have been fitted to a Legendre-polynomial expansion with $l = 0$, 1, and 2 up to 320 MeV/c and with $l = 0$ to 4 above 320 MeV/c. Curves resulting from the fits are shown in Fig. 8, and the coefficients are listed with the diagonal errors[9] in

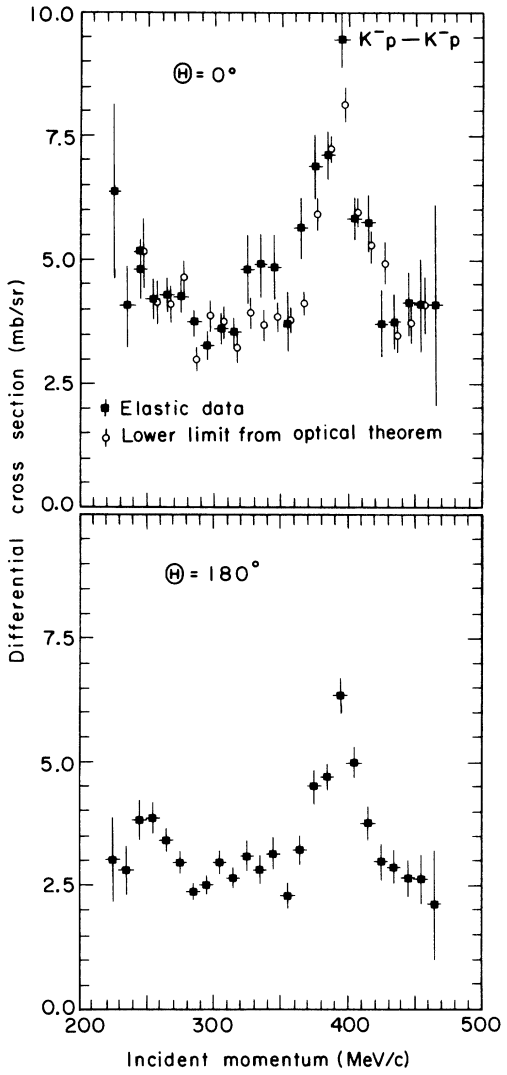

FIG. 11. Differential cross sections (mb/sr) at 0° and 180° for the elastic scattering $K^-p \to K^-p$. The squares are based on the measurements of the cross sections and the Legendre-polynomial fits to the angular distributions. The open circles represent the square of the imaginary part of the forward-scattering amplitude obtained from the optical theorem and the total K^-p cross sections.

Table V and are plotted in Fig. 9. The data of Watson *et al.*[3] and Armenteros *et al.*[10] are shown for comparison. The dramatic behavior in A_2/A_0 from the $\Lambda(1520)$ peaks higher than the data of Watson *et al.* The poorer momentum resolution of Watson *et al.* diminished the sharper structure we observe. We see a small amount of A_3/A_0 above 420 MeV/c, in agreement with Armenteros, and little or no significant A_4/A_0. The A_1/A_0 coefficient shows structure in the region of the $\Lambda(1520)$ arising from interference between the resonance D wave and a small P-wave background. Our data fall significantly below those of Armenteros at the high-energy end. The diagonal statistical errors are plotted in Fig. 9, and in several places the points show a larger scatter than would be expected on the basis of a low number of partial waves and statistics alone. However, there does not appear to be systematic behavior suggesting a resonance, and the large scatter is probably due to remaining systematic biases and/or overparametrization.

The elastic cross sections are shown in Fig. 10 and listed in Table III. The data of Sakitt *et al.*,[11] Kim,[12] Watson *et al.*,[3] and Armenteros *et al.*[10] are shown for comparison. Our data agree well with those of Watson and with the other experiments at the ends of our momentum coverage. We observe about a 5-mb enhancement at 395 MeV/c, in rough agreement with the charge-exchange enhancement with the $\Lambda(1520)$.

Figure 11 shows the elastic differential cross section at 0° and 180°. These have been predicted from the Legendre-polynomial coefficients and the cross section. No Coulomb corrections have been applied to the data. The circles on the 0° data are lower limits based on the optical theorem. These limits are the square of the imaginary part of the forward-scattering amplitude calculated by using the total K^-p cross section described in the following section. Within statistics, the cross sections are either equal to or greater than the limits.

C. Total K^-p cross section

Analysis has been made now of events from this exposure of all the kinematically possible final states. The results for the $\Sigma\pi$, $\Lambda\pi\pi$, $\Sigma\pi\pi$, $\Lambda\pi$, $\Lambda\gamma$, and $\Sigma\gamma$ final states are described in Ref. 1. We have summed the cross sections for these final states; the resulting total K^-p cross section is shown as a function of incident momentum in Fig. 12, and is listed in Table III. Shown for comparison are the results of Watson *et al.*[3] and Armenteros *et al.*[10] The $\Lambda(1520)$ gives about a 35-mb enhancement. The only other possible structure occurs in the region near 285 MeV/c. The cross section for every final state appears to be lower than those at the surrounding momenta, and thus the total cross section shows this same effect. We believe this is probably due to a fluctuation in the path length which is used in the cross section for each channel. The effect represents a fluctuation of about four standard deviations in the number τ decays used to determine the path length.

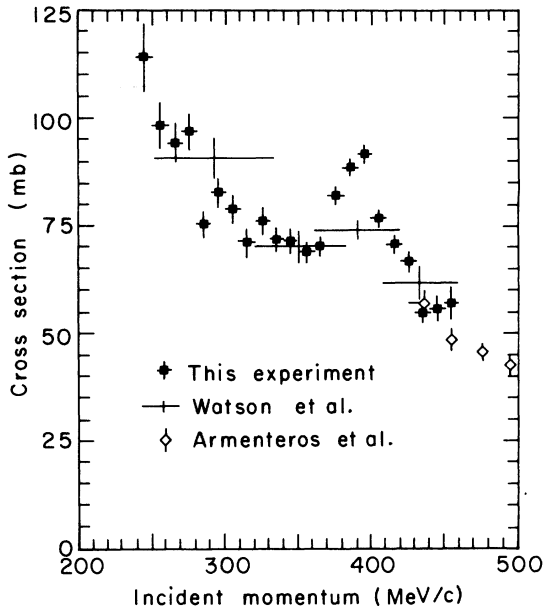

FIG. 12. Total K^-p cross section (mb) versus incident K^- momentum (MeV/c).

*Work done under the auspices of the U. S. Energy Research and Development Administration.

[1]Analyses of the $\Lambda\pi^+\pi^-$, $\Sigma\pi\pi$, $\Lambda\gamma$ and $\Sigma^0\gamma$, and $\Lambda\pi^0$ and $\Sigma^0\pi^0$ final states have been published: T. S. Mast, M. Alston-Garnjost, R. O. Bangerter, A. S. Barbaro-Galtieri, F. T. Solmitz, and R. D. Tripp, Phys. Rev. D 7, 5 (1973); 7, 3212 (1973); Phys. Rev. Lett. 21, 1715 (1968); Phys. Rev. D 11, 3078 (1975). Analysis of the $\Sigma^\pm\pi^\mp$ final states is in progress.

[2]R. O. Bangerter, Lawrence Berkeley Laboratory Alvarez Group Physics Note No. 574, 1965 (unpublished).

[3]M. G. Watson, M. Ferro-Luzzi, and R. D. Tripp, Phys. Rev. 131, 2248 (1963).

[4]T. S. Mast, L. K. Gershwin, M. Alston-Garnjost, R. O. Bangerter, A. Barbaro-Galtieri, J. J. Murray, F. T. Solmitz, and R. D. Tripp, Phys. Rev. 183, 1200 (1969).

[5]Particle Data Group, Phys. Lett. 50B, 1 (1974).
[6]S. E. Derenzo and R. H. Hildebrand, Nucl. Instrum. Methods 69, 287 (1969); R. Bangerter, Lawrence Berkeley Laboratory Alvarez Group Physics Note No. 731, 1971 (unpublished).
[7]D. Berley, S. P. Yamin, R. R. Kofler, A. Mann, G. W. Meisner, S. S. Yamamoto, J. Thompson, and W. Willis, Phys. Rev. D 1, 1996 (1970).
[8]R. Bangerter, Lawrence Berkeley Laboratory Alvarez Group Physics Note (unpublished).
[9]Full error matrices for the cross sections and Legendre coefficients presented here will appear in Lawrence Berkeley Laboratory Report No. LBL-3853 (unpublished).
[10]R. Armenteros, P. Baillon, C. Bricman, M. Ferro-Luzzi, E. Pagiola, J. O. Petersen, D. E. Plane, N. Schmitz, E. Burkhardt, H. Filthuth, E. Kluge, H. Oberlack, R. R. Ross, R. Barloutaud, P. Granet, J. Meyer, J. P. Porte, and J. Prevost, Nucl. Phys. B21, 15 (1970).
[11]M. Sakitt, T. S. Day, R. G. Glasser, N. Seeman, J. Friedman, W. E. Humphrey, and R. R. Ross, Phys. Rev. 139, B719 (1965).
[12]J. K. Kim, Columbia University Nevis Laboratories Report No. NEVIS-149, 1966 (unpublished).